European Heart Journal – Cardiovascular Imaging
doi:10.1093/ehjci/jew153

Optimization of coronary optical coherence tomography imaging using the attenuation-compensated technique: a validation study

Jing Chun Teo[1,2†], Nicolas Foin[1,2†*], Fumiyuki Otsuka[3,4], Heerajnarain Bulluck[1,2], Jiang Ming Fam[1], Philip Wong[1], Fatt Hoe Low[5], Hwa Liang Leo[2], Jean-Martial Mari[6], Michael Joner[3], Michael J.A. Girard[2,7], and Renu Virmani[3]

[1]National Heart Research Institute Singapore, National Heart Centre Singapore, 5 Hospital Drive, Singapore 169609; [2]Department of Biomedical Engineering and Duke-NUS Medical School, National University Singapore, Singapore; [3]CV Path Institute, Gaithersburg, MD, USA; [4]National Cerebral and Cardiovascular Center, Osaka, Japan; [5]Department of Cardiology, National University Heart Center, Singapore; [6]University of French Polynesia, French Polynesia; and [7]Singapore Eye Research Institute Singapore National Eye Centre, Singapore

Received 31 May 2016; accepted after revision 28 June 2016

Purpose To optimize conventional coronary optical coherence tomography (OCT) images using the attenuation-compensated technique to improve identification of plaques and the external elastic lamina (EEL) contour.

Method The attenuation-compensated technique was optimized via manipulating contrast exponent C, and compression exponent N, to achieve an optimal contrast and signal-to-noise ratio (SNR). This was applied to 60 human coronary lesions (38 native and 22 stented) *ex vivo* conventional coronary OCT images acquired from heart autopsies of 10 patients and matching histology was available as reference. Three independent reviewers assessed the conventional and attenuation-compensated OCT images blindly for plaque characteristics and EEL detection. Conventional OCT and compensated OCT assessment were compared against histology.

Results Using an optimized algorithm, the attenuation-compensated OCT images had a 2-fold improvement in contrast between different tissues in both stented and non-stented epicardial coronaries ($P < 0.05$). Overall sensitivity and specificity for plaque classification increased from 84 to 89% and from 92 to 94%, respectively, with substantial agreement among the three reviewers (Fleiss' Kappa *k*, 0.72 and 0.71, respectively). Furthermore, operators were 2.5 times more likely to identify the EEL contour in the attenuation-compensated OCT images ($k = 0.72$) than in the conventional OCT images ($k = 0.36$).

Conclusion The attenuation-compensated technique can be retrospectively applied to conventional OCT images and improves the detection of plaque characteristics and the EEL contour. This approach could complement conventional OCT imaging in the evaluation of plaque characteristics and quantify plaque burden in the clinical setting.

Introduction

In vivo intracoronary plaque characterization is now possible to aide decision-making in the cardiac catheterization laboratory at the time of percutaneous coronary intervention with the availability of intravascular ultrasound (IVUS) and optical coherence tomography (OCT) in the clinical setting. Although the axial resolution of OCT is 10 times superior than that of IVUS, the technique is limited by the rapid attenuation of the backscattering near-infrared signal in tissue, resulting in typical penetration depth of ~1–3 mm.[1–3] The use of intracoronary OCT remains low in routine clinical practice[4] as visualization of deep tissue structures such as the external elastic lamina (EEL) and atherosclerotic plaques morphology interpretation are both hampered by the low penetration depth and presence of shadow artifacts.[2] With the EEL contour of the diseased vessel not clearly visible, errors in measuring plaque burden are

† First authors.
* Corresponding author. Tel: +65 67042210. Email: nicolas.foin@gmail.com

more likely.[5,6] Consequently, the use of OCT has been mainly limited to the measurement of minimal luminal cross-sectional area, the detection of thin-cap fibroatheroma (TCFA), the assessment of stent expansion and strut apposition and dissection flap identification, and strut neo-endothelialization and healing response at follow-up.[2]

Attenuation-compensated OCT imaging was previously introduced by Girard *et al.* by correcting light attenuation to enhance contrast and penetration depth for ophthalmic OCT images.[7,8] We previously adapted this approach for conventional coronary OCT images.[9] The aim of this study was to optimize the contrast and signal-to-noise ratio (SNR) of conventional coronary OCT images using the attenuation-compensated technique and, using histology as reference, to compare the performance of the attenuation-compensated OCT images against the conventional OCT images in plaque and EEL detection.

Material and methods

Ex vivo OCT imaging and co-localized histology

The 10 autopsied hearts included in this study were from a previously published study investigating the vascular response to stenting by optical frequency domain imaging.[10] In brief, autopsied hearts were obtained from 10 patients. Initial coronary angiography was performed to identify vessels with >30% stenosis in diameter. A frequency domain OCT catheter (Terumo Corporation, Tokyo, Japan) was then introduced in these selected coronary arteries and sequential images were acquired using a pullback speed of 10 mm/s (frame rate 160 frames/s). Imaged coronary arterial frames were co-registered to histological sections using side branches as index markers and longitudinal and circumferential adjustments were made using anatomical landmarks such as calcification and luminal configuration. Imaged coronary arteries were then segmented at 3 mm intervals, processed and stained as previously described.[11]

OCT image enhancement using compensation

Compensation is an OCT post-processing technique that assumes light attenuation and backscattered light are proportional; and that A-scan signals will be fully attenuated at infinite depth.[7] Using this method, pixel intensity is theoretically amplified based on equation (1) without depth limitation. The amplification produces a compensated image, $I_{i,j}^{\mathrm{Comp}}$ which enhances 'weak signals' and is progressively increased with depth. Here, $1/\sum_{k=i}^{P} I_{i,j}^{c}$ is the amplification factor for each A-scan ($i = 0$: top of image; $i = \mathrm{P}$: bottom of image); C is an exponent that controls contrast.[7] The raw OCT frames were extracted from OCT pullbacks and post-processed with this algorithm in Matlab (Mathworks, USA) (*Figure 1*).

$$I_{i,j}^{\mathrm{Comp}} \frac{I_{i,j}^{c}}{2\sum_{k=i}^{P} I_{i,j}^{c}}. \tag{1}$$

While undesirable noise over-amplification maybe be induced using this method, as observed in ophthalmic OCT images, it is overcome by adaptive compensation which limits over-amplification in deep tissues.[8,12] Coronary OCT images do not face this problem as signal is often fully attenuated before such depth and has been demonstrated to considerably improve conventional coronary OCT image quality with image post-processing by compensation alone.[9,13]

Parameter optimization and contrast analysis

Ophthalmic and coronary tissues have very different optical properties. Light penetration depth is relatively larger in ophthalmic tissue since it is less attenuated and scattered. Thus, amount of contrast and pixel range for image analysis needed would be significantly different for coronary OCT image acquisition, let alone the application of the compensation technique. Application of an optimal set of compensation parameters would therefore be essential to improve contrast and accuracy of interpretation of these images by professionals.

The compensation parameter optimization was done by analysing the contrast and signal-to-noise ratio (SNR)[14] of 20 region of interests (ROIs) from three different patients' OCT images using varying configuration of contrast exponent, C, and compression exponent N, as described previously.[7,8] Higher C would enhance contrast and noise while higher N would increase the dynamic range of the image and they were varied between 2 and 3, and between 4 and 6, respectively. The same ROIs were marked on the OCT images for comparison of contrast and SNR between (i) intima/media, (ii) intima/plaque, and (iii) adventitia/plaque. Using equations (2) and (3), compensation parameters were optimized to provide the best overall contrast with ideal SNR.[7] According to the Rose criterion, an SNR of at least five is needed to be able to distinguish image features with 100% certainty.[15]

$$\mathrm{Contrast} = \left|\frac{I_1 - I_2}{I_1 + I_2}\right|, \tag{2}$$

where I_1 is the mean image intensity of the first ROI and I_2 the mean image intensity of the second ROI that is being compared. The contrast value can take a range of values from 0 to 1 with 1 representing maximal contrast and 0 representing least contrast

$$SNR = \frac{\mu}{\sigma}, \tag{3}$$

where μ is the mean signal intensity and σ is the standard deviation of the ROI.

After optimization of the compensation parameters, comparison with conventional OCT images were performed by evaluating contrast in the same ROI in both conventional and attenuation-compensated OCT images. Interlayer contrast and SNR were computed for (i) media/adventitia, (ii) plaque/non-plaque and (iii) neointima/intima. The mean tissue index was computed by normalizing intensity of histology-matched plaque ROIs to lumen intensity of the OCT images.

Evaluation of histology, conventional and attenuation-compensated OCT for cross-sectional images

All histology slides were reviewed by experienced readers and classified using the modified American Heart Association classification scheme[16,17] as follows:

Adaptive intimal thickening (AIT) or fibrous plaque: defined as lesions with predominantly fibrous tissue and no lipid pool.

Pathologic intimal thickening (PIT): defined as lesions with lipid pools but without apparent necrosis.

Thick-cap fibroatheroma (Th-FA): defined as plaques containing early or late necrotic core with a variable number of macrophages and lymphocytes infiltration present but with fibrous cap thickness >65 μm.

Vulnerable plaque or thin-cap fibroatheroma (TCFA): defined as fibroatheroma with the thinnest fibrous cap thickness ≤65 μm.

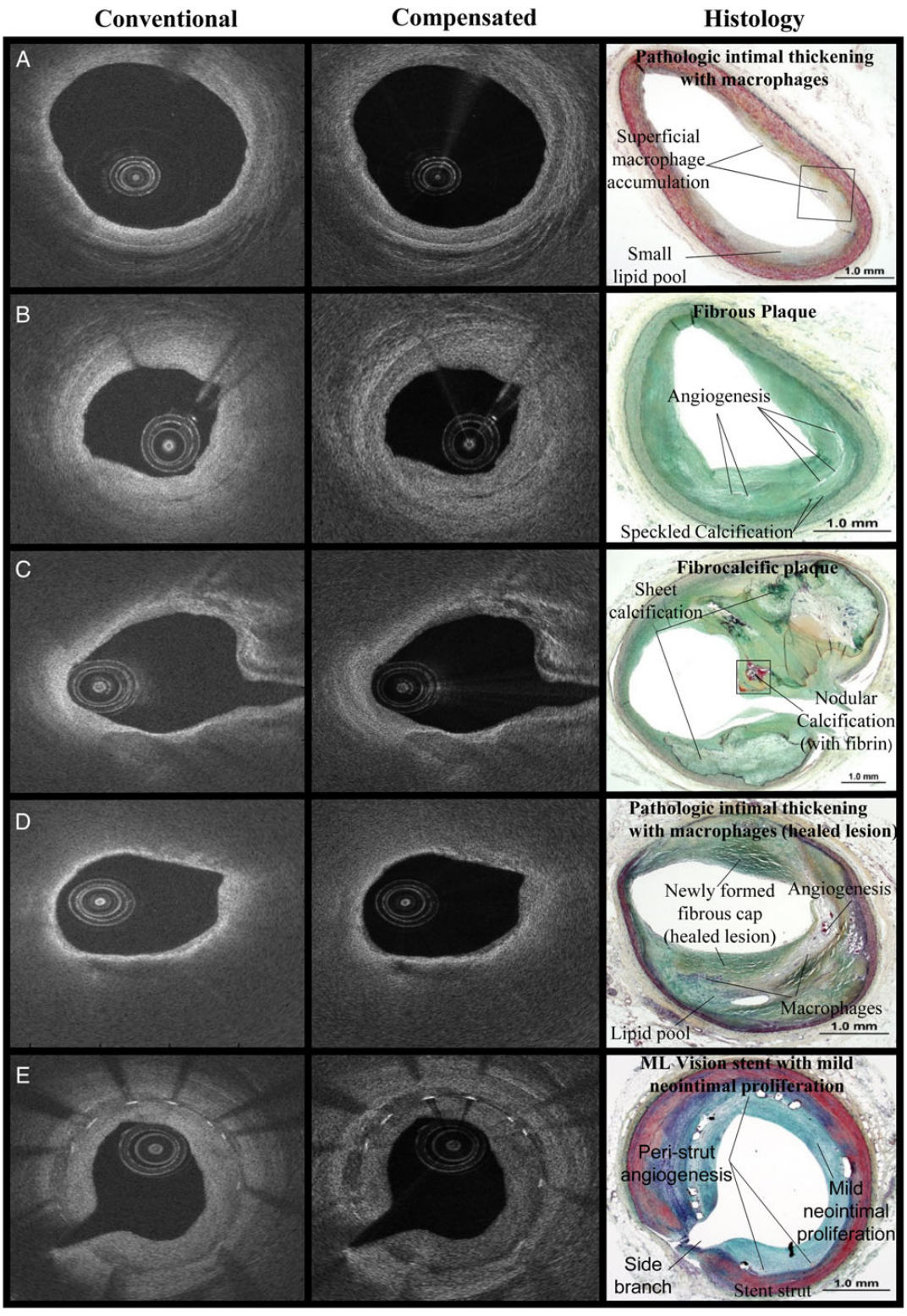

Figure 1 Comparison of conventional and attenuation-compensated OCT to histology. Optimized compensation (middle column) was performed on conventional OCT images (left column) and compared with matched histological images (right column) showing the following pathologies: row (*A*) pathologic intimal thickening (PIT) with macrophages, row (*B*) fibrous plaque, row (*C*) fibrocalcific plaque (calcified fibroatheroma with nodular calcification), row (*D*) pathologic intimal thickening (PIT) with macrophages (healed lesion) and row (*E*) ML vision stent with mild neointimal proliferation. Plaque type classification and description are indicated on histology images for clarity and it can be observed that structures are more clearly distinguished after compensation. Figure (*A*)–(*D*) were obtained from the right coronary artery (RCA), left anterior descending (LAD), LAD, left obtuse marginal (LOM), and RCA, respectively, from five separate patients.

Fibrocalcific plaque: defined as burnt-out lesions with severe calcification and absence or the presence of fractions of a necrotic core.

Three independent experienced reviewers blinded to the histological diagnosis were recruited to identify plaque types and assess EEL contour individually.

The following definitions were used to identify plaque morphology from OCT images[18–20]:

Fibrous plaque: defined as homogeneous, signal-rich regions with low attenuation.

Lipid-rich plaque: defined as signal-poor regions with diffuse borders.

Calcific plaque: defined as well-delineated, signal-poor regions with sharp borders.

A correct classification by OCT was considered only if it matched histological classification as below:

- Fibrous plaque matched with AIT/fibrous plaque or PIT with minor lipid present.
- Lipid-rich plaque matched with Th-FA, TCFA, or PIT with predominantly lipid present.
- Calcific plaque matched with fibrocalcific plaque.

EEL contour identification was considered successful when the full contour was discernible after accounting from signal dropouts from the catheter and stent struts.

Statistical analysis

Contrast and SNR between conventional and attenuation-compensated ROI values were compared using paired sample *t*-test for parametric variables or Wilcoxon Rank sum test for non-parametric variables. Using histology as the gold standard, sensitivity, specificity, and accuracy were computed based on their classification by OCT pre- and post-attenuation-compensation by the three reviewers. Their performances for the identification of the full EEL contour on the conventional and attenuation-compensated OCT images were assessed using McNemar test. Inter-observer variability was also computed via Fleiss' Kappa to assess reliability of agreement. All statistical analyses were performed using GraphPad Prism version 7 for Windows (GraphPad Software, La Jolla, CA, USA, www.graphpad.com) with $P < 0.05$ representing statistical significance.

Results

The baseline characteristics of the included subjects and histological plaque morphology classification are summarized in *Table 1*. The mean age of the subjects was 56.7 ± 14.6 years old and 8/10 died of a sudden cardiac cause. Of the 12 arteries harvested, there were 7 left anterior descending arteries, 4 right coronary arteries, and 1 circumflex artery. There were a total of 60 histological sections with 38 native lesions and 22 stented lesions with matching OCT images.

Parameter optimisation

From *Figure 2A* and *B*, an increase in C increased contrast but decreased SNR. Increasing N however had an opposite effect to increasing C. Although higher C (such as C = 3) gave better contrast, the corresponding SNR was too low. According to the Rose criteria,[15] an SNR of 3 would provide ~60% image certainty. C = 2, N = 4 was ultimately chosen even though SNR was <5 but a 15% drop in certainty was acceptable for a 2-fold increment in overall contrast.

Table 1 Patient and lesion characteristics

Patient ($n = 10$)		
Age (years)	56.7 ± 14.6	
Male gender	9	90%
Hypertension	9	90%
Hyperlipidaemia	2	20%
Diabetes mellitus	3	30%
Smoking	2	20%
Cause of death		
Sudden cardiac death	8	80%
Non-cardiac death	2	20%
Vessels ($n = 12$)		
LAD	7	58%
LCX	1	8%
RCA	4	33%
Non-stented lesions ($n = 38$)		
PIT macrophages poor	10	26%
PIT with macrophages	5	13%
Early fibroatheroma	3	8%
Late fibroatheroma	8	21%
Thin-cap fibroatheroma	3	8%
Fibrous plaque	3	8%
Fibrocalcific plaque	6	16%
Stented lesions ($n = 22$)		
Mild neointimal proliferation	17	77%
Moderate neointimal proliferation	4	18%
Heavily calcified neointima	1	5%

LAD, left anterior descending artery; LCx, left circumflex artery; RCA, right coronary artery.

Contrast and SNR

Analysis of 67 ROIs using the above optimized parameters from 10 different patients' OCT images showed an improvement in contrast between the conventional OCT images and the attenuation-compensated OCT images (media/adventitia contrast: 0.09 ± 0.04 vs. 0.16 ± 0.06, $P = 0.007$; plaque/non-plaque contrast: 0.06 ± 0.05 vs. 0.14 ± 0.06, $P = 0.002$; neointima/intima contrast in stented sections: 0.08 ± 0.05 vs. 0.17 ± 0.07, $P < 0.0001$). Overall, there was a two-fold increase in contrast regardless of the interlayer comparison (*Figure 2C*) but at the expense of a decrease in SNR from 7.7 ± 1.0 to 4.1 ± 0.5, $P < 0.0001$, between the conventional and attenuation-compensated OCT images.

Mean tissue index

Intra-plaque morphology in native lesions was better identifiable in attenuation-compensated OCT images than in conventional OCT images (*Figure 2D*). Lipid, calcific, and fibrous plaques were found to be associated with a mean tissue index of 5.2 ± 0.7, 7.2 ± 1.3, 8.6 ± 2.2 [lipid vs. calcific ($P = 0.0023$), lipid vs. fibrous ($P < 0.0001$) fibrous vs. calcific ($P = 0.16$)] after compensation and 1.7 ± 0.3, 1.7 ± 0.2, 2.6 ± 0 [lipid vs. calcific ($P = 0.87$), lipid vs. fibrous ($P < 0.0001$) fibrous vs. calcific ($P < 0.0001$)] before compensation, respectively.

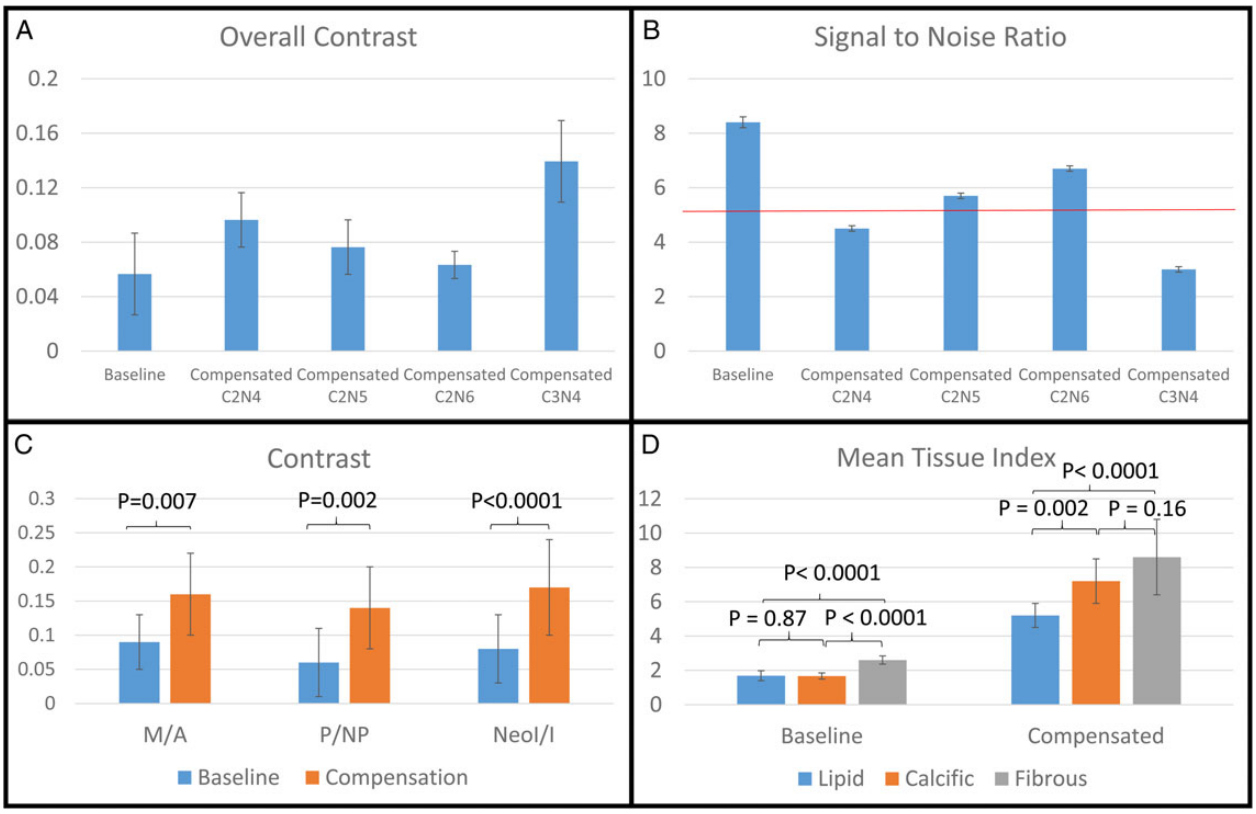

Figure 2 Contrast, signal to noise ratio & tissue Index analysis. (*A*) Overall contrast and (*B*) SNR in different configuration of contrast exponent, *C*, and compression exponent, N, were tabulated to sieve out best parameters for compensation. The red line in (*B*) represents SNR = 5; described by the Rose criterion as the minimum value to distinguish 100% feature certainty. Using optimized compensation parameters, (*C*) describes the interlayer contrast between (1) M/A to visualize EEL, (2) P/NP region to visualize contours of various plaque types, and (3) NeoI/I to visualize neointimal hyperplasia. The symbols denote Media, Adventitia, Plaque, Non-Plaque, Neointima, and Intima, respectively. The quantification of mean tissue intensity with respective to lipid-rich, calcific, and fibrous plaque types (*D*) signifies the ability for the attenuation-compensated technique to characterize a specific range of intensity for each plaque type instead of the attenuation coefficient.

Plaque morphology classification by OCT

Plaque classification showed that sensitivity and specificity obtained for fibrous, lipid and calcific plaques were 70% /97%, 93% /74% and 75% /95%, respectively, by conventional OCT images and 85% /96%, 90% /88%, 94% /97% by the attenuation-compensated OCT images (*Table 2*). Overall, there was a slight improvement in sensitivity and specificity for plaque classification from the conventional to the compensated OCT images [sensitivity: 84 vs. 89%; specificity: 92 vs. 94%]. Furthermore, full EEL contour was 2.5 times more easily identifiable ($k = 0.72$) in compensated images than baseline ($k = 0.36$, $P < 0.0001$) (*Figure 3A* and *B*).

Discussion

The major findings from our study are: (i) optimization of the attenuation-compensated technique for coronary OCT images provided a 2-fold increase in image contrast, at the expense of a reduction in SNR, but could still provide >80% image certainty as described by the Rose criteria[15]; (ii) application of the optimized attenuation-compensated algorithm retrospectively to conventional OCT images could differentiate between lipid-rich and calcific plaques based on different mean tissue index, which on conventional OCT images have similar signal-poor regions and the differentiation mainly rely on the borders definition; (iii) finally, there was improved readers' detection of plaque characteristics as defined by histology and also an improvement in the detection of the EEL contours, with good inter-reader concordance (*Figure 4*).

The diagnostic performance of the conventional OCT images for plaque detection as assessed by our three readers are in line with previous reports by Yabushita *et al.*[21] who did an *in vitro* OCT study of >300 human atherosclerotic artery segments and other studies.[18,19,22,23] These results build on previous reports[9,13] on the feasibility to apply the attenuation-compensated technique to coronary OCT images to improve plaque detection. Furthermore, we have provided histological validation to confirm an improvement in plaque detection and EEL contour delineation with the attenuation-compensated OCT images.

There are several potential important clinical impacts from the application of this post-processing technique to conventional

Table 2 **Expert classification on plaque characterization**

Detection	PPV (95% CL)	NPV (95% CL)	Sensitivity (95% CL)	Specificity (95% CL)	Accuracy
Fibrous					
Baseline	**0.95** (0.73–0.99)	**0.90** (0.81–0.95)	**0.70** (0.50–0.92)	**0.97** (0.92–0.99)	**0.91**
Compensated	**0.90** (0.73–0.97)	**0.93** (0.84–0.97)	**0.85** (0.67–0.94)	**0.96** (0.87–0.99)	**0.92**
Lipid/fibroatheroma					
Baseline	**0.83** (0.72–0.91)	**0.89** (0.73–0.96)	**0.93** (0.83–0.98)	**0.74** (0.59–0.86)	**0.85**
Compensated	**0.89** (0.76–0.95)	**0.90** (0.78–0.96)	**0.90** (0.78–0.96)	**0.88** (0.76–0.95)	**0.89**
Calcific					
Baseline	**0.75** (0.47–0.92)	**0.95** (0.88–0.99)	**0.75** (0.47–0.92)	**0.95** (0.88–0.99)	**0.92**
Compensated	**0.85** (0.61–0.96)	**0.99** (0.93–1.00)	**0.94** (0.71–0.99)	**0.97** (0.89–1.00)	**0.96**
Overall					
Baseline	**0.85** (0.76–0.91)	**0.92** (0.87–0.95)	**0.84** (0.76–0.91)	**0.92** (0.87–0.95)	**0.90**
Compensated	**0.88** (0.80–0.94)	**0.95** (0.90–0.97)	**0.89** (0.81–0.94)	**0.94** (0.90–0.97)	**0.93**

Assessment of plaque type was done by three independent experts. Using histology as control, respective responses were compared and tabulated for both conventional and compensated OCT images. Positive predictive value (PPV), negative predictive value (NPV), sensitivity, specificity, and accuracy, along with their respective 95% confidence level, are calculated for fibrous, lipid-rich, and calcific plaques. Overall predictive values calculated showed better identification of plaque type using compensated images.

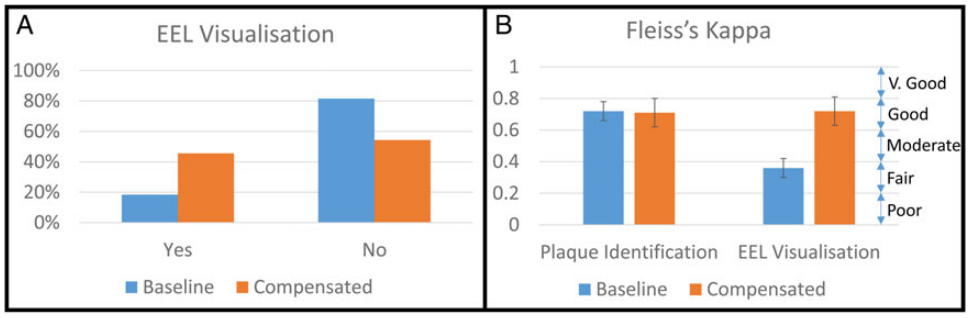

Figure 3 Expert classification on EEL identification. Binary [Yes/No] answers were collected from classification responses on the visualization of full EEL in conventional and attenuation-compensated images (*A*). Reliability of agreement between raters was computed using Fleiss Kappa (*B*).

OCT images. First of all, it can be retrospectively applied to existing OCT images and does not require additional data acquisition. Attenuation-compensated OCT improves EEL delineation and could improve plaque burden quantification for risk stratification. Detection of the EEL contour also allows the quantification of the severity of epicardial stenosis[24,25] where current visualization, unlike IVUS, interpretation of the EEL by conventional OCT is greatly impeded by rapid signal attenuation.[5,6] As a result, stent sizing may also be affected.[26] The lack of depth penetration has been shown to result in greater stent underexpansion and more geographic miss with OCT than with IVUS.[27] With improved tissue contrast of deeper structures, attenuation-compensated OCT may improve lesion and vessel sizing that would help with optimal stent selection and placement.

Vulnerable plaque features include a thin fibrous cap $<65\ \mu m$ overlaying a lipid-rich necrotic core (*Figure 1D*) that can be compromised via inflammation or mechanical forces.[28] Identification of such lipid-laden plaques, th-FA, before the advanced stages such as TCFA would be important. Many prospective studies have employed OCT to study these features to establish the efficacy of statin therapy[29–31] or dietary modification[30] in stabilizing plaques to improve clinical outcomes.[32] However, even though fibrous cap thickness can be reliably measured by OCT, such morphology alone may be insufficient to identify vulnerable lesions. Attenuation-compensated OCT offers the prospect to improve the detection of lipid-rich plaques underlying thin-capped fibrous plaques and to better assess response to medications aiming at stabilizing plaques.

Several studies have attempted to quantify tissue attenuation to better identify tissue/plaque differentiation from coronary OCT images.[33–35] These methods are not easy to apply because they require fitting OCT A-scan signal to predefined exponential decay models.[34,36] Moreover, to implement such technique requires accurate segmentation of vessel/plaque contours.[35] Identifying such conformations, however, is restricted by rapid signal attenuation. In addition, evidence of multiple scattering may cause a higher signal than predicted by the decay model, depending on the beam parameters and tissue optical properties.[37,38] The attenuation-compensated technique offers an easy alternative approach since the output image is correlated to tissue attenuation[7] and has been

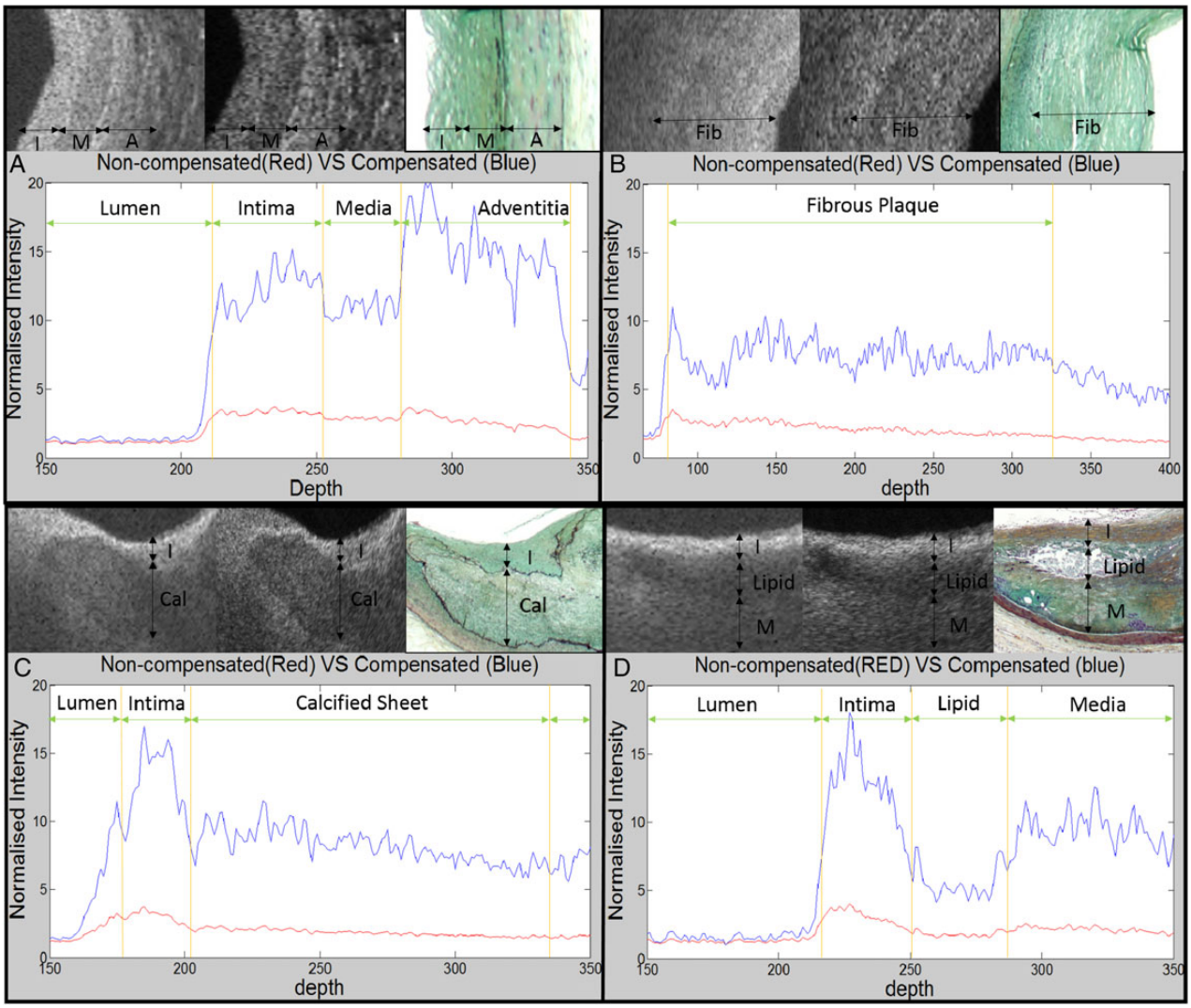

Figure 4 OCT A-line representation of tissue intensity. OCT A-line normalized (to the lumen) before (red line) and after compensation (blue line). The graphical representation showed enhanced signal contrast between different layer structures (Intima/Media/Adventitia) in compensated images to increase visibility through blood vessel depth (*A*). Each layer and plaque type had a corresponding range of normalized signal intensity for identification. (*B*–*D*) shows how signal intensity varies based on plaque type, (*B*) contains fibrous plaque, (*C*) contains a calcified sheet, and (*D*) contains a lipid plaque. (*A*)–(*D*) were matched to histology images for verification and demarcated accordingly.

shown to be effective with simple homogenous materials.[39] With our modification, we are able to quantify plaque types better based on the mean tissue index with good reproducibility.

Limitations

This was a small study of 10 patients only and OCT was performed *ex vivo*. However, we were able to provide human histological validation for 60 lesions and showed the improved plaque detection following attenuation compensation in both stented and native lesions. This technique also led to a reduction in SNR but was still within acceptable limits. Although some plaques were heterogeneous with a mixture of lipid-rich, calcific, and fibrous plaques, we elected to classify them as predominantly lipid-rich, calcific, and fibrous only by OCT for simplicity in this proof-of-concept study. Whether this technique performs better than conventional OCT images for *in vivo* images and may improve risk stratification needs to be tested in future adequately powered clinical studies.

Conclusion

In this study, we applied an optimized attenuation-compensated algorithm to enhance coronary OCT images and we have shown an improvement in image contrast and provided histological validation for the detection of plaque characteristics and the EEL contour. This approach could complement conventional OCT imaging in the evaluation of plaque characteristics and burden in the clinical setting.

Conflict of interest: M.J. and R.V. are employees of CV path. N.F., J-M.M. and M.J.A.G. hold IP related to the OCT compensation technique in Cardiology.

References

1. Bezerra HG, Costa MA, Guagliumi G, Rollins AM, Simon DI. Intracoronary optical coherence tomography: a comprehensive review clinical and research applications. *JACC Cardiovasc Interv* 2009;**2**:1035–46.
2. Gutiérrez-Chico JL, Alegría-Barrero E, Teijeiro-Mestre R, Chan PH, Tsujioka H, de Silva R *et al.* Optical coherence tomography: from research to practice. *Eur Heart J Cardiovasc Imaging* 2012;**13**:370–84.
3. Otsuka F, Joner M, Prati F, Virmani R, Narula J. Clinical classification of plaque morphology in coronary disease. *Nat Rev Cardiol* 2014;**11**:379–89.
4. Members WC, Levine GN, Bates ER, Blankenship JC, Bailey SR, Bittl JA *et al.* 2011 ACCF/AHA/SCAI guideline for percutaneous coronary intervention: a report of the American College of Cardiology Foundation/American Heart Association Task Force on Practice Guidelines and the Society for Cardiovascular Angiography and Interventions. *Circulation* 2011;**124**:e574–651.
5. Prati F, Guagliumi G, Mintz GS, Costa M, Regar E, Akasaka T *et al.* Expert review document part 2: methodology, terminology and clinical applications of optical coherence tomography for the assessment of interventional procedures. *Eur Heart J* 2012;**33**:2513–20.
6. Roleder T, Jąkała J, Kałuża GL, Partyka Ł, Proniewska K, Pociask E *et al.* The basics of intravascular optical coherence tomography. *Adv Intervent Cardiol* 2015;**11**:74–83.
7. Girard MJA, Strouthidis NG, Ethier CR, Mari JM. Shadow removal and contrast enhancement in optical coherence tomography images of the human optic nerve head. *Invest Ophthalmol Vis Sci* 2011;**52**:7738.
8. Mari JM, Strouthidis NG, Park SC, Girard MJA. Enhancement of lamina cribrosa visibility in optical coherence tomography images using adaptive compensation. *Invest Ophthalmol Vis Sci* 2013;**54**:2238.
9. Lee R, Foin N, Otsuka F, Wong P, Mari J-M, Joner M *et al.* Intravascular assessment of arterial disease using compensated OCT in comparison with histology. *JACC Cardiovasc Imaging* 2016;**9**:321–2.
10. Nakano M, Vorpahl M, Otsuka F, Taniwaki M, Yazdani SK, Finn AV *et al.* Ex vivo assessment of vascular response to coronary stents by optical frequency domain imaging. *JACC Cardiovasc Imaging* 2012;**5**:71–82.
11. Nakano M, Yahagi K, Yamamoto H, Taniwaki M, Otsuka F, Ladich ER *et al.* Additive value of integrated backscatter IVUS for detection of vulnerable plaque by optical frequency domain imaging: an ex vivo autopsy study of human coronary arteries. *JACC Cardiovasc Imaging* 2016;**9**:163–72.
12. Girard MJ, Ang M, Chung CW, Farook M, Strouthidis N, Mehta JS *et al.* Enhancement of corneal visibility in optical coherence tomography images using corneal adaptive compensation. *Transl Vis Sci Technol* 2015;**4**:3.
13. Foin N, Mari JM, Nijjer S, Sen S, Petraco R, Ghione M *et al.* Intracoronary imaging using attenuation-compensated optical coherence tomography allows better visualisation of coronary artery diseases. *Cardiovasc Revasc Med* 2013;**14**:139–43.
14. Liu X, Kang JU. Sparse OCT: optimizing compressed sensing in spectral domain optical coherence tomography. *Proc SPIE* 2011;**7904**:874058.
15. Bushberg JT. *The Essential Physics of Medical Imaging*. Philadelphia: Wolters Kluwer Health/Lippincott Williams & Wilkins, 2012.
16. Virmani R, Kolodgie FD, Burke AP, Farb A, Schwartz SM. Lessons from sudden coronary death: a comprehensive morphological classification scheme for atherosclerotic lesions. *Arterioscler Thromb Vasc Biol* 2000;**20**:1262–75.
17. Yahagi K, Kolodgie FD, Otsuka F, Finn AV, Davis HR, Joner M *et al.* Pathophysiology of native coronary, vein graft, and in-stent atherosclerosis. *Nat Rev Cardiol* 2016;**13**:79–98.
18. Kume T, Akasaka T, Kawamoto T, Watanabe N, Toyota E, Neishi Y *et al.* Assessment of coronary arterial plaque by optical coherence tomography. *Am J Cardiol* 2006;**97**:1172–5.
19. Rieber J, Meissner O, Babaryka G, Reim S, Oswald M, Koenig A *et al.* Diagnostic accuracy of optical coherence tomography and intravascular ultrasound for the detection and characterization of atherosclerotic plaque composition in ex-vivo coronary specimens: a comparison with histology. *Coronary Artery Dis* 2006;**17**:425–30.
20. Tearney GJ, Regar E, Akasaka T, Adriaenssens T, Barlis P, Bezerra HG *et al.* Consensus standards for acquisition, measurement, and reporting of intravascular optical coherence tomography studies: a report from the International Working Group for Intravascular Optical Coherence Tomography Standardization and Validation. *J Am College Cardiol* 2012;**59**:1058–72.
21. Yabushita H, Bouma BE, Houser SL, Aretz HT, Jang I-K, Schlendorf KH *et al.* Characterization of human atherosclerosis by optical coherence tomography. *Circulation* 2002;**106**:1640–5.
22. Guo J, Sun L, Chen YD, Tian F, Liu HB, Chen L *et al.* [Ex vivo assessment of coronary lesions by optical coherence tomography and intravascular ultrasound in comparison with histology results]. *Zhonghua xin xue guan bing za zhi* 2012;**40**:302–6.
23. Kawasaki M, Bouma BE, Bressner J, Houser SL, Nadkarni SK, MacNeill BD *et al.* Diagnostic accuracy of optical coherence tomography and integrated backscatter intravascular ultrasound images for tissue characterization of human coronary plaques. *J Am College Cardiol* 2006;**48**:81–8.
24. Jansen CHP, Onthank DC, Cuello F, Botnar RM, Wiethoff AJ, Warley A *et al.* Assessment of atherosclerotic plaque burden with an elastin-specific magnetic resonance contrast agent. *Nat Med* 2011;**17**:383–8.
25. von Birgelen C, Hartmann M. Coronary plaque burden and cardiovascular risk factors: single-point versus serial assessment. *J Am College Cardiol* 2006;**48**:1914–5.
26. Kubo T, Akasaka T, Shite J, Suzuki T, Uemura S, Yu B *et al.* OCT compared with IVUS in a coronary lesion assessment: the OPUS-CLASS study. *JACC Cardiovasc Imaging.* 2013;**6**:1095–1104.
27. Habara M, Nasu K, Terashima M, Kaneda H, Yokota D, Ko E *et al.* Impact of frequency-domain optical coherence tomography guidance for optimal coronary stent implantation in comparison with intravascular ultrasound guidance. *Circ Cardiovasc Interven* 2012;**5**:193.
28. Virmani R, Burke AP, Kolodgie FD, Farb A. Pathology of the thin-cap fibroatheroma: a type of vulnerable plaque. *J Intervent Cardiol* 2003;**16**:267–72.
29. Takarada S, Imanishi T, Kubo T, Tanimoto T, Kitabata H, Nakamura N *et al.* Effect of statin therapy on coronary fibrous-cap thickness in patients with acute coronary syndrome: assessment by optical coherence tomography study. *Atherosclerosis* 2009;**202**:491–7.
30. Hattori K, Ozaki Y, Ismail TF, Okumura M, Naruse H, Kan S *et al.* Impact of statin therapy on plaque characteristics as assessed by serial OCT, grayscale and integrated backscatter–IVUS. *JACC: Cardiovasc Imaging* 2012;**5**:169–77.
31. Nishio R, Shinke T, Otake H, Nakagawa M, Nagoshi R, Inoue T *et al.* Stabilizing effect of combined eicosapentaenoic acid and statin therapy on coronary thin-cap fibroatheroma. *Atherosclerosis* 2014;**234**:114–9.
32. Sinclair H, Bourantas C, Bagnall A, Mintz GS, Kunadian V. OCT for the identification of vulnerable plaque in acute coronary syndrome. *JACC: Cardiovasc Imaging* 2015;**8**:198–209.
33. Tearney GJ, Yabushita H, Houser SL, Aretz HT, Jang I-K, Schlendorf KH *et al.* Quantification of macrophage content in atherosclerotic plaques by optical coherence tomography. *Circulation* 2003;**107**:113–9.
34. van Soest G, Goderie T, Regar E, Koljenović S, van Leenders GL, Gonzalo N *et al.* Atherosclerotic tissue characterization in vivo by optical coherence tomography attenuation imaging. *J Biomed Opt* 2010;**15**:011105.
35. Xu C, Schmitt JM, Carlier SG, Virmani R. Characterization of atherosclerosis plaques by measuring both backscattering and attenuation coefficients in optical coherence tomography. *J Biomed Opt* 2008;**13**:034003.
36. van der Meer FJ, Faber DJ, Sassoon DMB, Aalders MC, Pasterkamp G, van Leeuwen TG. Localized measurement of optical attenuation coefficients of atherosclerotic plaque constituents by quantitative optical coherence tomography. *IEEE Trans Med Imaging* 2005;**24**:1369–76.
37. Schmitt JM, Knuttel A, Yadlowsky M, Eckhaus MA. Optical-coherence tomography of a dense tissue: statistics of attenuation and backscattering. *Phys Med Biol* 1994;**39**:1705.
38. Karamata B, Laubscher M, Leutenegger M, Bourquin S, Lasser T, Lambelet P. Multiple scattering in optical coherence tomography. I. Investigation and modeling. *J Opt Soc Am A* 2005;**22**:1369–79.
39. Vermeer KA, Mo J, Weda JJA, Lemij HG, de Boer JF. Depth-resolved model-based reconstruction of attenuation coefficients in optical coherence tomography. *Biomed Opt Express* 2014;**5**:322.